
Function-Space Empirical Bayes Regularisation with Student’s t Priors

Pengcheng Hao¹

Ercan Engin Kuruoglu¹

¹Institute of Data and Information, Tsinghua Shenzhen International Graduate School, Shenzhen, China

Abstract

Bayesian deep learning (BDL) has emerged as a principled approach to produce reliable uncertainty estimates by integrating deep neural networks with Bayesian inference, and the selection of informative prior distributions remains a significant challenge. Various function-space variational inference (FSVI) regularisation methods have been presented, assigning meaningful priors over model predictions. However, these methods typically rely on a Gaussian prior, which fails to capture the heavy-tailed statistical characteristics inherent in neural network outputs. By contrast, this work proposes a novel function-space empirical Bayes regularisation framework—termed ST-FS-EB—which employs heavy-tailed Student’s t priors in both parameter and function spaces. Also, we approximate the posterior distribution through variational inference (VI), inducing an evidence lower bound (ELBO) objective based on Monte Carlo (MC) dropout. Furthermore, the proposed method is evaluated against various VI-based BDL baselines, and the results demonstrate its robust performance in in-distribution prediction, out-of-distribution (OOD) detection and handling distribution shifts.

1 INTRODUCTION

The remarkable predictive accuracy of deep neural networks (DNNs) has established them as the cornerstone of modern artificial intelligence. Yet, a closer examination reveals a fundamental blind spot: a DNN, no matter how accurately it predicts, remains oblivious to what it does not know Gawlikowski et al. [2023]. This distinction between "knowing" and "knowing that one knows" lies at the heart of intelligent decision-making. In high-stakes environments, a model’s silence about its own uncertainty—e.g., failing to

flag misdiagnosis risks in medical imaging Lambert et al. [2024] or misjudging pedestrian presence in autonomous driving Wang et al. [2025]—represents not merely a technical limitation but a practical hazard. The question then is not only how to make predictions but also how to equip models with the capacity to express doubt. Bayesian neural networks (BNNs) offer a principled response to this challenge Jospin et al. [2022]. By casting network weights as random variables governed by prior distributions and pursuing posterior inference, BNNs move beyond point estimates to produce predictions together with uncertainty. To infer the posterior distribution over weights, researchers have explored a variety of approaches, including Markov Chain Monte Carlo (MCMC), Laplace approximation, and variational inference (VI). Most BNNs employ Gaussian priors, yet both network parameters and predictive distributions often exhibit heavy-tailed behaviour in practice Fortuin et al. [2022]. To accommodate this heavy-tailed behaviour, recent works have adopted heavy-tailed distributions as priors for the model weights Fortuin et al. [2021], Xiao et al. [2023], Harrison et al. [2025]. However, these weight-space methods struggle to incorporate meaningful prior knowledge into BNNs, as the relationship between weights and predictions is highly intricate.

An alternative paradigm shifts inference from weight space to function space. Instead of placing priors on model parameters, functional VI (FVI) Sun et al. [2019] defines interpretable prior distributions directly over model predictions and optimises a functional evidence lower bound (ELBO). However, this conceptual shift comes at a cost: the Kullback–Leibler (KL) divergence between infinite-dimensional stochastic processes lacks a closed-form expression. Sun et al. [2019] approximates the KL divergence with the spectral Stein gradient estimator (SSGE) Shi et al. [2018], introducing significant computational overhead and limiting the scalability of the FVI in real-world settings. By contrast, linearisation-based function-space VI (FSVI) Rudner et al. [2022] methods impose Gaussian priors on model parameters and approximate the induced functional distribution as a

Gaussian process (GP). This yields a tractable, closed-form approximation of the KL divergence between prior and posterior Immer et al. [2021], Rudner et al. [2022], Cinquin and Bamler [2024]. However, the linearisation strategy, though convenient, distorts the true function mapping and imposes a heavy computational burden due to the need to evaluate Jacobian matrices. By contrast, the function-space empirical Bayes (FS-EB) approach Rudner et al. [2023, 2024a] introduces regularisation simultaneously in both parameter and function spaces, circumventing the need for linearisation. However, all these functional methods are built upon Gaussian assumptions, limiting their ability to adequately model heavy-tailed behaviour.

In comparison, this work considers a new FS-EB framework based on Student’s t priors (ST-FS-EB). The benefits are twofold: 1) the heavy-tailed nature of the Student’s t distribution provides enhanced robustness to outliers and model misspecification compared to the Gaussian distribution; 2) the additional degree-of-freedom (dof) parameter offers greater flexibility in capturing the tail decay of the true underlying distribution. The main contributions of this work are shown below:

1. We present a Student’s t prior-based FS-EB framework, which employs an empirical functional prior derived from Student’s t -distributed weights and a functional likelihood defined by a Student’s t process.
2. We adopt Monte Carlo (MC) dropout as the variational distribution to approximate the posterior within a VI framework, deriving an MC dropout-based ELBO objective.
3. Our method is compared against a range of function-space and parameter-space regularisation baselines on five real-world benchmarks. The results demonstrate that ST-FS-EB achieves robust performance under both standard and distribution-shift settings.

The remainder of this paper is organised as follows. Section 2 reviews the related work, while Section 3 presents the theoretical background. Section 4 then introduces the proposed ST-FS-EB method. The experimental evaluation is reported in Section 5, and Section 6 concludes the paper.

2 RELATED WORK

2.1 WEIGHT-SPACE VARIATIONAL INFERENCE REGULARISATION

Hinton and Van Camp [1993] pioneers the first variational Bayesian approach for neural networks, using a diagonal Gaussian approximation of the weight posterior to implement minimum description length (MDL) regularisation. Also, Graves [2011] extends the variational method to complex neural network architectures by estimating the gra-

dients of model parameters via MC sampling. However, both methods require substantial computational costs, making them impractical for large-scale neural networks. By contrast, Kingma and Welling [2014] introduces a reparameterization trick, which enables straightforward optimisation of the variational ELBO using standard stochastic gradient methods. Then Blundell et al. [2015] introduces a Bayes by Backprop method, a VI algorithm compatible with backpropagation that learns distributions over model weights by minimising the ELBO. Building upon this line of research, Gal and Ghahramani [2016] proposes the MC dropout method, establishing a theoretical connection between dropout training and approximate Bayesian inference.

2.2 FUNCTION-SPACE VARIATIONAL INFERENCE REGULARISATION

Initial FSVI studies focus on directly approximating posterior distributions over functions induced by neural networks. In particular, Wang et al. [2019] proposes a function-space particle optimisation framework, performing VI over regression functions. Also, Flam-Shepherd et al. [2017] presents a function-space prior alignment approach that maps GP priors to BNN priors, allowing BNNs to inherit structured functional properties from GPs. Additionally, Sun et al. [2019] demonstrates that the KL divergence between infinite-dimensional prior and variational functional processes can be expressed as the supremum of marginal KL divergences over all finite input sets, which allows the functional ELBO to be approximated using finite measurement sets. However, the employed SSGE method requires high computational cost, and the function-space variational objective is generally ill-defined Burt et al. [2021]. By contrast, an efficient VI framework for posterior approximation is enabled by Ma et al. [2019] through the use of functional implicit stochastic process priors to handle intractable function-space objectives. Also, a well-defined variational objective is achieved in Ma and Hernández-Lobato [2021] through a grid-functional KL divergence built on stochastic process generators. In comparison, Khan et al. [2019], Immer et al. [2021] formulate a VI objective by modelling DNNs as GPs using Laplace and GGN approximations. To enable variance parameter optimisation, Rudner et al. [2022] further introduces a fully BNN-based FSVI framework, in which the KL divergence is rendered finite by defining the prior as the pushforward of a Gaussian distribution in weight space. Moreover, Cinquin and Bamler [2024] proposes an interpretable prior construction based on a pretrained GP prior and introduces a regularised KL divergence to ensure a well-defined variational objective. However, these approaches approximate the model output distribution through linearisation, which requires computationally expensive Jacobian evaluations and simultaneously introduces additional approximation error. In comparison, the FS-EB approach Rudner et al. [2023, 2024b,c] avoids linearisation and constructs

an empirical functional prior by combining a weight-space prior with a GP-based functional likelihood.

3 PRELIMINARY

This section presents the fundamental concepts that form the foundation of our proposed ST-FS-EB framework. Specifically, Section 3.1 and Section 3.2 introduce the Student’s t distribution and the Student’s t process, respectively. Furthermore, Section 3.3 describes the FS-EB framework, which serves as the basis for our method.

3.1 THE STUDENT’S T DISTRIBUTION

The Student’s t distribution Ahsanullah et al. [2014] is a continuous probability distribution, which can be viewed as a heavy-tailed generalisation of the Gaussian distribution and provides increased robustness to outliers. A univariate Student’s t random variable $x \in \mathbb{R}$ with location parameter $\mu \in \mathbb{R}$, scale parameter $\sigma > 0$ and dof $\nu > 0$ is denoted by $x \sim \mathcal{ST}(\nu, \mu, \sigma^2)$. Its probability density function (PDF) is given by

$$p(x) = \frac{\Gamma(\frac{\nu+1}{2})}{\Gamma(\frac{\nu}{2})\sqrt{\pi\nu\sigma^2}} \left(1 + \frac{(x-\mu)^2}{\nu\sigma^2}\right)^{-\frac{\nu+1}{2}}, \quad (1)$$

where $\Gamma(\cdot)$ denotes the Gamma function. Compared with the Gaussian distribution, the polynomial decay of the tails in (1) assigns significantly higher probability mass to extreme events. Smaller values of ν correspond to heavier tails, implying higher robustness to outliers. Also, the Student’s t distribution includes the Gaussian distribution as a limiting special case. Specifically, as the dof parameter $\nu \rightarrow \infty$, the Student’s t distribution converges to a normal distribution:

$$\mathcal{ST}(\nu, \mu, \sigma^2) \xrightarrow{\nu \rightarrow \infty} \mathcal{N}(\mu, \sigma^2).$$

This property establishes a smooth continuum between heavy-tailed and Gaussian modelling, allowing the Student’s t distribution to adaptively interpolate depending on the dof value ν . Besides, assume a random vector $\mathbf{x} \in \mathbb{R}^d$ follows a multivariate Student’s t distribution Shah et al. [2014], i.e. $\mathbf{x} \sim \mathcal{MVT}(\nu, \boldsymbol{\mu}, \mathbf{K})$, with the dof value $\nu > 2$, mean $\boldsymbol{\mu} \in \mathbb{R}^d$, covariance matrix $\mathbf{K} \in \mathbb{R}^{d \times d}$, its density can be written as

$$p(\mathbf{x}) = \frac{\Gamma(\frac{\nu+d}{2})}{\Gamma(\frac{\nu}{2})((\nu-2)\pi)^{d/2}|\mathbf{K}|^{-1/2}} \times \left(1 + \frac{(\mathbf{x}-\boldsymbol{\mu})^\top \mathbf{K}^{-1}(\mathbf{x}-\boldsymbol{\mu})}{\nu-2}\right)^{-\frac{\nu+d}{2}}.$$

3.2 THE STUDENT’S T PROCESS

The Student’s t process (TP) Shah et al. [2014], Solin and Särkkä [2015] is a heavy-tailed, nonparametric distribution

over functions and can be viewed as a robust generalisation of the GP Seeger [2004]. A stochastic process g defined on an input space \mathcal{X} is called a Student’s t process with dof $\nu > 2$, mean function $\Phi : \mathcal{X} \rightarrow \mathbb{R}$, and kernel function $k : \mathcal{X} \times \mathcal{X} \rightarrow \mathbb{R}$, denoted by $g \sim \mathcal{TP}(\nu, \Phi, k)$, if for any finite set of inputs $\mathbf{x} = \{x_1, \dots, x_\eta\}$,

$$(g(x_1), \dots, g(x_\eta))^\top \sim \mathcal{MVT}(\nu, \boldsymbol{\mu}, \mathbf{K}), \quad (2)$$

where $\boldsymbol{\mu}_\alpha = \Phi(x_\alpha)$, $\mathbf{K}_{\alpha\beta} = k(x_\alpha, x_\beta)$ and $\alpha, \beta = 1, \dots, \eta$. Also, $\mathcal{MVT}(\nu, \boldsymbol{\mu}, \mathbf{K})$ can be written in a Gaussian scale mixture (GSM) form Solin and Särkkä [2015]. Let $\gamma^{-1} \sim \Gamma(\nu/2, (\nu-2)/2)$ denote a latent inverse-Gamma scale variable and

$$g(\mathbf{x}) \mid \gamma \sim \mathcal{N}(\phi, \gamma \mathbf{K}), \quad (3)$$

then marginalising over γ yields the Student’s t process in Eq. (2). As the dof parameter $\nu \rightarrow \infty$, the Student’s t process converges to a GP:

$$\mathcal{TP}(\nu, \Phi, k) \xrightarrow{\nu \rightarrow \infty} \mathcal{GP}(\Phi, k).$$

Due to its heavy-tailed marginals, the Student’s t process assigns higher probability to extreme function values than a GP, leading to improved robustness against outliers.

3.3 FUNCTION-SPACE EMPIRICAL BAYES REGULARISATION

This section describes the FS-EB framework Rudner et al. [2023, 2024a], which combines parameter-space and function-space regularisation. The FS-EB method considers a supervised learning setting defined by a dataset

$$\mathcal{D} = \left\{x_{\mathcal{D}}^{(n_{\mathcal{D}})}, y_{\mathcal{D}}^{(n_{\mathcal{D}})}\right\}_{n_{\mathcal{D}}=1}^{N_{\mathcal{D}}} = (\mathbf{x}_{\mathcal{D}}, \mathbf{y}_{\mathcal{D}}).$$

where the $N_{\mathcal{D}}$ samples are independently and identically distributed. The inputs satisfy $x_{\mathcal{D}}^{(n_{\mathcal{D}})} \in \mathcal{X} \subseteq \mathbb{R}^D$, and the corresponding outputs lie in a target space $y_{\mathcal{D}}^{(n_{\mathcal{D}})} \in \mathcal{Y}$. For regression tasks, the target space is continuous with $\mathcal{Y} \subseteq \mathbb{R}^L$, whereas for L -class classification problems, the targets are represented as L -dimensional binary vectors, i.e., $\mathcal{Y} \subseteq \{0, 1\}^L$. The FS-EB defines an auxiliary posterior as an empirical prior, i.e.,

$$p(\boldsymbol{\theta} \mid \mathbf{y}_c, \mathbf{x}_c) \propto p(\mathbf{y}_c \mid \mathbf{x}_c, \boldsymbol{\theta}) p(\boldsymbol{\theta}). \quad (4)$$

where $(\mathbf{x}_c, \mathbf{y}_c) = \left\{x_c^{(n_c)}, y_c^{(n_c)}\right\}_{n_c=1}^{N_c}$ denotes a set of context points and $p(\boldsymbol{\theta})$ represents the prior distribution over the parameters. Moreover, to formulate the likelihood function $p(\mathbf{y}_c \mid \mathbf{x}_c, \boldsymbol{\theta})$, FS-EB adopts a linear model

$$z(\mathbf{x}_c) \doteq h(\mathbf{x}_c; \phi_0) \boldsymbol{\Psi} + \boldsymbol{\epsilon}, \quad (5)$$

where $h(\cdot; \phi_0)$ is a feature extractor with parameter ϕ_0 , $\boldsymbol{\Psi} \sim \mathcal{N}(\mathbf{0}, \tau_1 I_1)$ and $\boldsymbol{\epsilon} \sim \mathcal{N}(\mathbf{0}, \tau_2 I_2)$. Also, I_1 and I_2

are identity matrices, and the positive scalars $\tau_1, \tau_2 \in \mathbb{R}^+$ govern the variances of the stochastic components. Give context point set \mathbf{x}_c , we have

$$p(z(\mathbf{x}_c) | \mathbf{x}_c) = \mathcal{N}(z(\mathbf{x}_c); \mathbf{0}, \mathbf{K}(\mathbf{x}_c, \mathbf{x}_c)),$$

with the covariance matrix

$$\mathbf{K}(\mathbf{x}_c, \mathbf{x}_c) = \tau_1 h(\mathbf{x}_c; \phi_0) h(\mathbf{x}_c; \phi_0)^\top + \tau_2 I_2. \quad (6)$$

Viewing this distribution as a likelihood over neural network outputs, FS-EB obtains the following formulation:

$$p(\mathbf{y}_c^l | \mathbf{x}_c, \theta) = \mathcal{N}(\mathbf{y}_c^l; [f(\mathbf{x}_c; \theta)]_l, \mathbf{K}(\mathbf{x}_c, \mathbf{x}_c)), \quad (7)$$

where $\mathbf{y}_c = \mathbf{0}$ and $f(\cdot; \theta)$ is the neural network parameterised by θ . Also, $[f(\mathbf{x}_c; \theta)]_l$ and \mathbf{y}_c^l ($l = 1, \dots, L$) are the l -th component of $f(\mathbf{x}_c; \theta)$ and \mathbf{y}_c , respectively. Then the auxiliary posterior can be expressed as

$$p(\theta | \mathbf{y}_c, \mathbf{x}_c) \propto p(\theta) \prod_{l=1}^L p(\mathbf{y}_c^l | \mathbf{x}_c, \theta). \quad (8)$$

Leveraging this auxiliary posterior as an empirical prior, the posterior over parameters given the full dataset is obtained via Bayes' rule:

$$p(\theta | \mathbf{y}_D, \mathbf{x}_D) \propto p(\mathbf{y}_D | \mathbf{x}_D, \theta) p(\theta | \mathbf{y}_c, \mathbf{x}_c). \quad (9)$$

For posterior approximation, Rudner et al. [2023, 2024a] introduce techniques grounded in maximum a posteriori (MAP) estimation and VI.

4 PROPOSED METHOD: ST-FS-EB

Following the introduction of the FS-EB framework, this section presents our proposed ST-FS-EB method. In particular, Section 4.1 introduces the empirical Student's t priors over functions, while Section 4.2 describes the corresponding empirical Bayes variational inference method for posterior approximation.

4.1 EMPIRICAL STUDENT'S T PRIORS OVER FUNCTIONS

Analogous to Eq. (4) in the FSEB framework, we introduce an auxiliary posterior conditioned on the context inputs \mathbf{x}_c , given by

$$p_{st}(\theta | \mathbf{y}_c, \mathbf{x}_c) \propto p_{st}(\mathbf{y}_c | \mathbf{x}_c, \theta) p_{st}(\theta),$$

where both the functional likelihood $p_{st}(\mathbf{y}_c | \mathbf{x}_c, \theta)$ and the parameter prior $p_{st}(\theta)$ are formulated under Student's t assumptions. Let $\theta_i, i = 1, \dots, \mathcal{I}$ is the i -th component of θ and N_θ is the number of parameters. We define an

independent and identically distributed (i.i.d.) prior over each model parameter as

$$p_{st}(\theta_i) = \mathcal{ST}(\theta_i; \nu_\theta, \mu_\theta, \sigma_\theta^2) \quad (10)$$

with zero mean, i.e., $\mu_\theta = 0$. Also, following the stochastic modelling strategy in (5), we construct the functional likelihood $p_{st}(\mathbf{y}_c | \mathbf{x}_c, \theta)$ by a stochastic model

$$z_{st}(\mathbf{x}_c) \doteq \sqrt{\gamma} (h(\mathbf{x}_c; \phi_0) \Psi + \epsilon),$$

where $h(\cdot; \phi_0)$, Ψ and ϵ have the same meaning as in (5), and $\gamma^{-1} \sim \Gamma(\nu_\theta/2, (\nu_\theta - 2)/2)$. Then we have

$$p(z_{st}(\mathbf{x}_c) | \gamma) = \mathcal{N}(z_{st}(\mathbf{x}_c); \mathbf{0}, \gamma \mathbf{K}(\mathbf{x}_c, \mathbf{x}_c)).$$

where $\mathbf{K}(\mathbf{x}_c, \mathbf{x}_c)$ can be calculated by (6). According to Eq. (2) and the GSM form in Eq. (3), we obtain

$$p_{st}(z_{st}(\mathbf{x}_c) | \mathbf{x}_c) = \mathcal{MVT}(z_{st}(\mathbf{x}_c); \nu_\theta, \mathbf{0}, \mathbf{K}(\mathbf{x}_c, \mathbf{x}_c)).$$

Treating $p_{st}(\mathbf{y}_c^l | \mathbf{x}_c, \theta)$ as the likelihood model for neural network outputs, we define

$$p_{st}(\mathbf{y}_c^l | \mathbf{x}_c, \theta) = \mathcal{MVT}(\mathbf{y}_c^l; \nu_\theta, [f(\mathbf{x}_c; \theta)]_l, \mathbf{K}(\mathbf{x}_c, \mathbf{x}_c)) \quad (11)$$

where $[f(\mathbf{x}_c; \theta)]_l$ and $\mathbf{y}_c^l = \mathbf{0}$ are the l -th component of $f(\mathbf{x}_c; \theta)$ and \mathbf{y}_c , respectively. Then we have the ST-FS-EB empirical prior

$$p_{st}(\theta | \mathbf{y}_c, \mathbf{x}_c) \propto \prod_{i=1}^{\mathcal{I}} p_{st}(\theta_i) \prod_{l=1}^L p_{st}(\mathbf{y}_c^l | \mathbf{x}_c, \theta). \quad (12)$$

Remark 1 *In the FS-EB framework, both the parameter prior and the functional likelihood are based on Gaussian assumptions. However, existing studies have shown that practical models often exhibit heavy-tailed behaviour in both parameter distributions and output responses Fortuin et al. [2022]. This empirical evidence motivates the adoption of our Student's t -based prior $p_{st}(\theta | \mathbf{y}_c, \mathbf{x}_c)$, providing a more robust and expressive Bayesian modelling framework.*

4.2 EMPIRICAL BAYES VARIATIONAL INFERENCE

This section formulates posterior inference for the proposed ST-FS-EB prior. In accordance with Eq. (9), the posterior distribution given the full dataset takes the form

$$p_{st}(\theta | \mathbf{y}_D, \mathbf{x}_D) \propto p(\mathbf{y}_D | \mathbf{x}_D, \theta) p_{st}(\theta | \mathbf{y}_c, \mathbf{x}_c).$$

Due to the intractability of the posterior distribution $p_{st}(\theta | \mathbf{x}_D, \mathbf{y}_D)$, we adopt VI to approximate the posterior. Specifically, we seek to minimise the KL divergence between a tractable variational distribution $q(\theta)$ and the posterior, i.e.,

$$\min_{q(\theta) \in \mathcal{Q}} D_{\text{KL}}(q(\theta) \| p_{st}(\theta | \mathbf{x}_D, \mathbf{y}_D)),$$

where \mathcal{Q} denotes a chosen family of tractable variational distributions. This variational optimisation problem is equivalently formulated as the maximisation of the ELBO:

$$\mathcal{L}(\boldsymbol{\theta}) = \mathbb{E}_{q(\boldsymbol{\theta})} [\log p(\mathbf{y}_{\mathcal{D}} | \mathbf{x}_{\mathcal{D}}, \boldsymbol{\theta})] - D_{\text{KL}}(q(\boldsymbol{\theta}) \| p_{st}(\boldsymbol{\theta} | \mathbf{y}_c, \mathbf{x}_c)) \quad (13)$$

where the first term corresponds to the expected data log-likelihood under the variational posterior, encouraging accurate data fitting. Besides, the second term acts as a regularisation term that constrains $q(\boldsymbol{\theta})$ to remain close to the proposed ST-FS-EB empirical prior $p_{st}(\boldsymbol{\theta} | \mathbf{y}_c, \mathbf{x}_c)$.

Variational approximation via MC dropout. We employ MC dropout Gal and Ghahramani [2016] to construct a tractable variational posterior $q(\boldsymbol{\theta})$. Each stochastic forward pass under a randomly sampled dropout mask yields a realisation $\boldsymbol{\theta}^{(s)} \sim q(\boldsymbol{\theta})$, with $\boldsymbol{\theta}^{(s)}$ denoting the effective parameters associated with the s -th dropout mask. According to (12) and (13), the objective can be approximated as

$$\hat{\mathcal{L}}(\boldsymbol{\theta}) \approx \frac{1}{S} \sum_{s=1}^S \left[\log p(\mathbf{y}_{\mathcal{D}} | \mathbf{x}_{\mathcal{D}}, \boldsymbol{\theta}^{(s)}) + \sum_{l=1}^L \log p_{st}(\mathbf{y}_c^l | \mathbf{x}_c, \boldsymbol{\theta}^{(s)}) \right] + \rho \sum_{i=1}^{\mathcal{I}} \log p_{st}(\theta_i)$$

where S denotes the number of MC samples and ρ is the MC dropout rate. Then, according to (1), (10), (11), we have

$$\begin{aligned} \hat{\mathcal{L}}(\boldsymbol{\theta}) \propto & \frac{1}{S} \sum_{s=1}^S \left[\log p(\mathbf{y}_{\mathcal{D}} | \mathbf{x}_{\mathcal{D}}, \boldsymbol{\theta}^{(s)}) \right. \\ & \left. - \frac{\nu_{\theta} + N_c}{2} \sum_{l=1}^L \log \left(1 + \frac{c([\mathbf{f}(\mathbf{x}_c; \boldsymbol{\theta}^{(s)})]_l, \mathbf{K}(\mathbf{x}_c, \mathbf{x}_c))}{\nu_{\theta} - 2} \right) \right] \\ & - \frac{\rho(\nu_{\theta} + 1)}{2} \sum_{i=1}^{\mathcal{I}} \log \left(1 + \frac{\theta_i^2}{\nu_{\theta} \sigma_{\theta}^2} \right) \end{aligned}$$

where $c(\mathbf{x}, \Sigma) \doteq \mathbf{x}^{\top} \Sigma^{-1} \mathbf{x}$ is the squared Mahalanobis distance between \mathbf{x} and the origin under covariance matrix Σ . The detailed proof is provided in Section A. For each epoch of optimisation, the training data $(\mathbf{x}_{\mathcal{D}}, \mathbf{y}_{\mathcal{D}})$ is randomly split into a partition of M equally-sized minibatch $(\mathbf{x}_B^{(m)}, \mathbf{y}_B^{(m)}) \sim (\mathbf{x}_{\mathcal{D}}, \mathbf{y}_{\mathcal{D}})$, where $m = 1, \dots, M$. Let $(\mathbf{x}_c^{(m)}, \mathbf{y}_c^{(m)}) \sim (\mathbf{x}_c, \mathbf{y}_c)$ denote the corresponding randomly sampled context points, we have the loss function at the m -th minibatch:

$$\begin{aligned} \hat{\mathcal{L}}^{(m)}(\boldsymbol{\theta}) \propto & \frac{1}{S} \sum_{s=1}^S \left[\log p(\mathbf{y}_B^{(m)} | \mathbf{x}_B^{(m)}, \boldsymbol{\theta}^{(s)}) \right. \\ & \left. - \frac{\nu_{\theta} + N_c^m}{2} \sum_{l=1}^L \log \left(1 + \frac{c([\mathbf{f}(\mathbf{x}_c^{(m)}; \boldsymbol{\theta}^{(s)})]_l, \mathbf{K}_c^{(m)})}{\nu_{\theta} - 2} \right) \right] \\ & - \frac{\rho(\nu_{\theta} + 1)}{2M} \sum_{i=1}^{\mathcal{I}} \log \left(1 + \frac{\theta_i^2}{\nu_{\theta} \sigma_{\theta}^2} \right) \end{aligned} \quad (14)$$

Algorithm 1: ST-FS-EB training process of each epoch

Initialisation: training data $(\mathbf{x}_{\mathcal{D}}, \mathbf{y}_{\mathcal{D}})$, model parameters $\boldsymbol{\theta}$, feature extractor $h(\cdot; \phi_0)$, MC dropout rate ρ , positive scalars τ_1, τ_2 , dof parameter ν_{θ} , scale parameter σ_{θ} , number of MC samples S , number of batches M , number of context samples N_c^m ,

for each minibatch $(\mathbf{x}_B^{(m)}, \mathbf{y}_B^{(m)}) \sim (\mathbf{x}_{\mathcal{D}}, \mathbf{y}_{\mathcal{D}})$:

1. Sample context points $(\mathbf{x}_c^{(m)}, \mathbf{y}_c^{(m)})$.
2. Compute loss $\hat{\mathcal{L}}^{(m)}(\boldsymbol{\theta})$ by (14).
3. Update parameters $\boldsymbol{\theta}$.

end for

where N_c^m is the sample size in $(\mathbf{x}_c^{(m)}, \mathbf{y}_c^{(m)})$ and $\mathbf{K}_c^{(m)} = \mathbf{K}(\mathbf{x}_c^{(m)}, \mathbf{x}_c^{(m)})$. Also, the last term is scaled by an extra factor $\frac{1}{M}$ as in Blundell et al. [2015].

Remark 2 *The original FS-EB framework assumes Gaussian priors and a Gaussian variational distribution, yielding a closed-form expression for the KL divergence between them. In contrast, our method employs heavy-tailed Student's t priors, which break this conjugacy and therefore preclude a closed-form KL divergence. To accommodate this choice, we leverage MC dropout to implicitly construct the variational posterior, enabling scalable and tractable posterior inference without requiring an explicit parametric form of $q(\boldsymbol{\theta})$.*

Selection of Priors. To construct the functional likelihood $p_{st}(\mathbf{y}_c | \mathbf{x}_c, \boldsymbol{\theta})$, we choose a feature extractor $h(x; \phi_0)$. In our approach, this extractor is a randomly initialised neural network, which naturally induces inductive biases over functions Wilson and Izmailov [2020]. We can also consider a pre-trained feature extractor when available, as in Rudner et al. [2023, 2024a].

Selection of Context Distributions. We select context points from an auxiliary dataset $(\mathbf{x}_c, \mathbf{y}_c)$ which is semantically related to but distributionally distinct from the training distribution. For instance, when training on CIFAR-10, we sample context points from CIFAR-100 to provide relevant OOD contextual information.

Posterior Predictive Distributions. At inference time, predictions are formed by averaging the outputs of multiple stochastic forward passes with dropout enabled, thereby approximating the predictive distribution via MC integration under the variational posterior $q(\boldsymbol{\theta})$

$$\begin{aligned} q(y^* | x^*) &= \int p(y^* | f(x^*; \boldsymbol{\theta})) q(\boldsymbol{\theta}) d\boldsymbol{\theta} \\ &\approx \frac{1}{\Xi} \sum_{\xi=1}^{\Xi} p(y^* | f(x^*; \boldsymbol{\theta}^{(\xi)})), \end{aligned}$$

Table 1: In-distribution prediction performance. **Best** results are in bold and second best are underlined.

Metric	Dataset	ST-FS-EB(our)	FS-EB	GFSVI	MC Dropout	MFVI	MAP
ACC \uparrow	MNIST	99.33 \pm 0.052	99.10 \pm 0.067	99.17 \pm 0.071	<u>99.32 \pm 0.035</u>	99.15 \pm 0.095	99.09 \pm 0.062
	FMNIST	92.38 \pm 0.194	90.49 \pm 0.218	91.97 \pm 0.099	<u>92.29 \pm 0.189</u>	90.28 \pm 0.281	91.87 \pm 0.242
	CIFAR-10	<u>86.52 \pm 0.395</u>	74.42 \pm 0.426	84.94 \pm 0.548	86.54 \pm 0.364	74.85 \pm 0.416	77.31 \pm 23.656
	PathMNIST	87.83 \pm 1.143	86.80 \pm 1.338	<u>88.32 \pm 1.087</u>	87.69 \pm 0.771	87.34 \pm 1.253	89.15 \pm 2.522
	OrganAMNIST	90.16 \pm 0.635	88.56 \pm 0.713	87.99 \pm 0.353	<u>89.81 \pm 0.560</u>	88.55 \pm 0.585	86.15 \pm 1.111
ECE \downarrow	MNIST	0.012 \pm 0.001	0.010 \pm 0.002	0.003 \pm 0.001	0.012 \pm 0.001	<u>0.008 \pm 0.001</u>	0.003 \pm 0.001
	FMNIST	0.038 \pm 0.003	0.013 \pm 0.003	0.012 \pm 0.002	0.038 \pm 0.004	<u>0.011 \pm 0.003</u>	0.012 \pm 0.003
	CIFAR-10	0.021 \pm 0.007	0.085 \pm 0.004	<u>0.023 \pm 0.004</u>	0.028 \pm 0.005	0.083 \pm 0.003	<u>0.023 \pm 0.012</u>
	PathMNIST	0.049 \pm 0.009	<u>0.024 \pm 0.007</u>	0.066 \pm 0.008	0.055 \pm 0.006	0.019 \pm 0.003	0.068 \pm 0.020
	OrganAMNIST	<u>0.026 \pm 0.007</u>	0.038 \pm 0.010	0.034 \pm 0.006	0.016 \pm 0.002	0.046 \pm 0.003	0.051 \pm 0.008
NLL \downarrow	MNIST	<u>0.028 \pm 0.001</u>	0.034 \pm 0.001	0.026 \pm 0.002	0.029 \pm 0.002	0.029 \pm 0.001	0.026 \pm 0.001
	FMNIST	0.226 \pm 0.005	0.263 \pm 0.005	<u>0.225 \pm 0.002</u>	0.227 \pm 0.004	0.269 \pm 0.006	0.231 \pm 0.005
	CIFAR-10	0.398 \pm 0.013	0.763 \pm 0.009	0.466 \pm 0.012	<u>0.399 \pm 0.010</u>	0.752 \pm 0.008	0.642 \pm 0.584
	PathMNIST	0.454 \pm 0.069	<u>0.405 \pm 0.044</u>	0.509 \pm 0.067	0.525 \pm 0.113	0.399 \pm 0.038	0.512 \pm 0.121
	OrganAMNIST	0.317 \pm 0.012	0.364 \pm 0.016	0.436 \pm 0.025	<u>0.318 \pm 0.016</u>	0.360 \pm 0.016	0.478 \pm 0.036

Table 2: Out-of-distribution detection performance. **Best** results are in bold and second best are underlined.

In	OOD	ST-FS-EB(our)	FS-EB	GFSVI	MC Dropout	MFVI	MAP
MNIST	FMNIST	99.86 \pm 0.057	100.00 \pm 0.000	<u>99.99 \pm 0.003</u>	98.59 \pm 0.351	98.60 \pm 0.231	98.56 \pm 0.255
	NotMNIST	<u>99.96 \pm 0.011</u>	99.99 \pm 0.003	99.99 \pm 0.006	96.86 \pm 0.286	94.06 \pm 0.777	95.43 \pm 0.670
	MNIST-c	89.38 \pm 0.569	90.90 \pm 0.665	<u>90.61 \pm 0.909</u>	84.60 \pm 0.679	82.69 \pm 0.943	82.30 \pm 0.743
FMNIST	MNIST	99.70 \pm 0.170	<u>99.63 \pm 0.116</u>	99.70 \pm 0.116	81.22 \pm 1.717	77.48 \pm 2.726	78.40 \pm 2.310
	NotMNIST	<u>96.23 \pm 0.665</u>	96.97 \pm 0.289	95.30 \pm 0.535	80.03 \pm 1.611	70.57 \pm 4.324	69.49 \pm 1.552
CIFAR-10	SVHN	84.87 \pm 2.269	82.53 \pm 1.836	88.96 \pm 1.524	<u>85.32 \pm 1.174</u>	82.56 \pm 2.690	82.70 \pm 11.716
	CIFAR-10C0	<u>55.34 \pm 0.429</u>	55.08 \pm 0.419	55.04 \pm 0.436	55.40 \pm 0.428	55.07 \pm 0.382	54.73 \pm 1.724
	CIFAR-10C2	<u>64.19 \pm 0.784</u>	61.71 \pm 0.870	63.72 \pm 0.942	64.49 \pm 0.842	61.69 \pm 0.794	62.52 \pm 4.470
	CIFAR-10C4	71.35 \pm 1.225	66.27 \pm 1.423	<u>71.53 \pm 1.362</u>	71.77 \pm 1.107	66.39 \pm 1.381	68.97 \pm 6.767
PathMNIST	BloodMNIST	97.29 \pm 0.957	85.85 \pm 10.503	<u>96.28 \pm 3.110</u>	71.24 \pm 13.143	78.38 \pm 7.713	81.05 \pm 7.870
OrganAMNIST	OrganSMNIST	<u>87.85 \pm 2.960</u>	86.13 \pm 1.015	88.45 \pm 1.601	79.80 \pm 0.608	77.73 \pm 0.564	74.85 \pm 1.058

where $\theta^{(\xi)} \sim q(\theta)$, Ξ denotes the number of MC samples used to estimate the predictive distribution. x^* and y^* denote a test input and its corresponding predicted output, respectively.

5 EXPERIMENTS

This section presents a comprehensive evaluation of ST-FS-EB, beginning with experimental descriptions—including baselines, setup and implementation details—followed by three sets of experiments: (1) in-distribution prediction and OOD detection (Section 5.1); (2) robustness under distribution shift (Section 5.2); (3) an ablation study on the dof values of the Student’s t prior (Section 5.3).

Baselines. We benchmark our method against a diverse set of baselines spanning both function-space and parameter-space regularisation paradigms. Specifically, we include two recent FSVI approaches: FS-EB Rudner et al. [2023] and generalised FSVI (GFSVI) Cinquin and Bamler [2024]. On the parameter-space side, we consider MC Dropout Gal

and Ghahramani [2016] and mean-field VI (MFVI) Blundell et al. [2015], along with parameter-space MAP estimation Bishop and Nasrabadi [2006] as a standard baseline.

Setup. We evaluate our method on five in-distribution datasets: MNIST, FashionMNIST (FMNIST), CIFAR-10, PathMNIST, and OrganAMNIST. For OOD detection evaluation, we use (1) FMNIST, NotMNIST and corrupted MNIST (MNIST-C) for MNIST; (2) MNIST and NotMNIST for FMNIST; (3) SVHN and corrupted CIFAR-10 with severity levels 0, 2, and 4 (denoted CIFAR-10C0, CIFAR-10C2, CIFAR-10C4) for CIFAR-10; (4) BloodMNIST for PathMNIST; (5) OrganSMNIST for OrganAMNIST. For MNIST-C and CIFAR-10C0/C2/C4, multiple corruption types are considered, and we report the average OOD detection scores across all corruption types as the final evaluation scores. For MNIST, FMNIST and OrganAMNIST, we employ a convolutional neural network consisting of two convolutional layers with 32 and 64 filters of size 3×3 , ending with a 128-unit fully connected layer. For CIFAR-10 and PathMNIST, we use a deeper architecture comprising six convolutional layers with 32, 32, 64, 64, 128, and 128 filters (all with 3×3

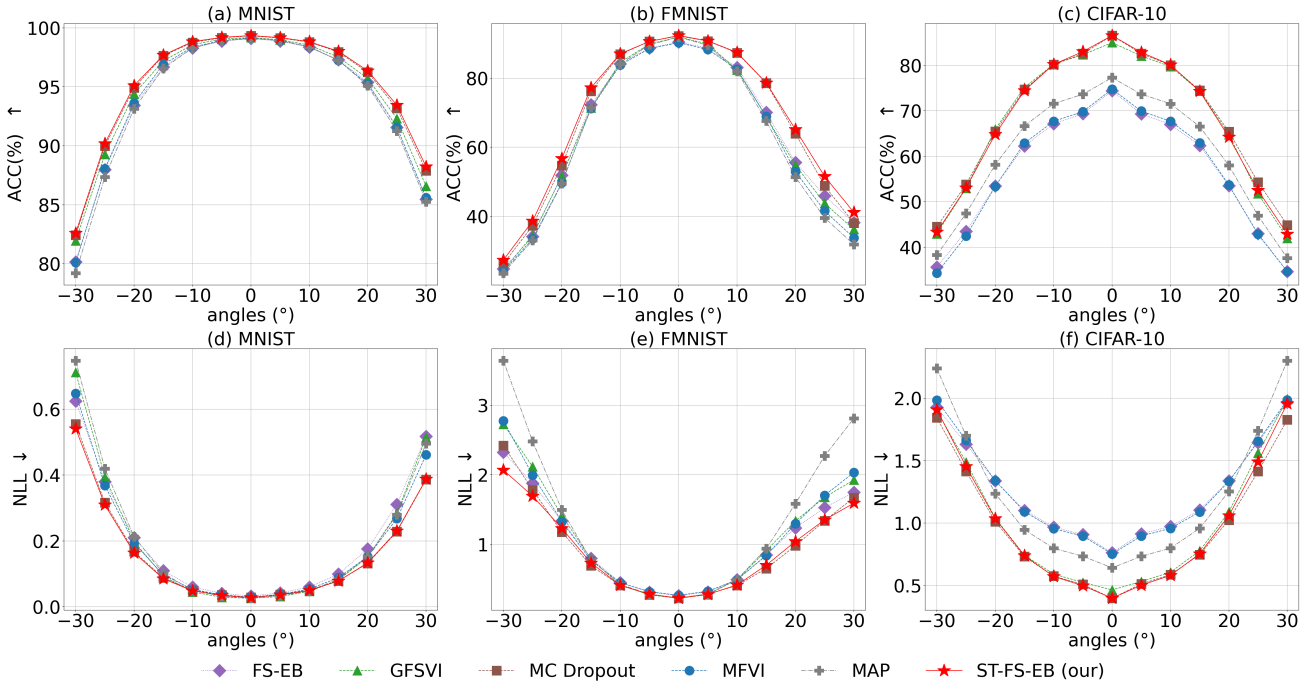


Figure 1: Performance under distribution shift induced by image rotations. The top row ((a)–(c)) reports ACC scores, while the bottom row ((d)–(f)) shows NLL. The horizontal axes denote the rotation angle, ranging from -30° to 30° , and the vertical axis shows the corresponding performance scores.

kernels), capped by a dense layer with 128 hidden units. All models are trained using the Adam optimiser, and all images are normalised to the range $[0, 1]$. For additional details on neural network architectures, hyperparameters and other settings, see Section B. In-distribution prediction performance is evaluated using classification accuracy (ACC), negative log-likelihood (NLL), and expected calibration error (ECE). For OOD detection, we use the area under the receiver operating characteristic curve (AUROC), with the maximum softmax probability (MSP) employed as the detection score.

Implementation. All experiments are conducted with 10 MC runs, and we report both the mean and standard deviation. For context construction, we use related auxiliary datasets: Kuzushiji-MNIST (KMNIST) for MNIST and FashionMNIST, CIFAR-100 for CIFAR-10, DermaMNIST for PathMNIST and OrganCMNIST for OrganAMNIST. Also, the feature extractor $h(\cdot; \phi_0)$ shares the same architecture as the trained neural network, except that the final layer is removed. Moreover, we set $S = 10$ for training and $\Xi = 10$ for inference.

5.1 PREDICTION AND OOD DETECTION PERFORMANCE

The in-distribution prediction and OOD detection results of our proposed ST-FS-EB, in comparison with all baseline methods, are shown in Table 1 and Table 2, respectively. As

shown in Table 1, ST-FS-EB achieves the highest ACC on MNIST, FMNIST, and OrganAMNIST, and remains competitive with the top-performing methods on CIFAR-10 and PathMNIST. In terms of ECE, ST-FS-EB performs competitively on CIFAR-10 and OrganAMNIST, but exhibits higher ECE values than some baselines (e.g., GFSVI and MFVI) on MNIST, FMNIST, and PathMNIST, suggesting its variability in calibration performance across datasets. With respect to NLL, ST-FS-EB consistently achieves the lowest values on FMNIST, CIFAR-10 and OrganAMNIST, while remaining comparable to that of the best-performing baselines. By contrast, Table 2 shows that ST-FS-EB consistently achieves the first- or second-best performance across most OOD benchmarks and remains close to the optimal results in the other cases.

Overall, ST-FS-EB achieves a strong balance between predictive accuracy and uncertainty estimation, with robust performance across datasets and metrics. It outperforms FS-EB and GFSVI in in-distribution accuracy while retaining competitive OOD detection. Also, the ST-FS-EB consistently surpasses MC Dropout, MFVI, and MAP on both prediction and OOD benchmarks in most cases.

5.2 PERFORMANCE ON DISTRIBUTION SHIFTS

To investigate the robustness of the proposed method under distribution shift, this experiment introduces controlled

Table 3: Influence of dof values of Student’s t priors. **Best** results are in bold and second best are underlined.

IN	Metric/OOD	2.1	3.0	5.0	10.0	20.0	Gaussian
MNIST	ACC	99.31 ± 0.031	99.31 ± 0.072	<u>99.33 ± 0.052</u>	99.34 ± 0.052	99.34 ± 0.058	99.31 ± 0.044
	NLL	0.031 ± 0.001	0.030 ± 0.002	<u>0.028 ± 0.001</u>	0.028 ± 0.002	0.027 ± 0.001	0.031 ± 0.001
	FMNIST	<u>99.91 ± 0.042</u>	99.85 ± 0.035	<u>99.86 ± 0.057</u>	<u>99.84 ± 0.040</u>	99.95 ± 0.016	99.90 ± 0.036
	NotMNIST	<u>99.96 ± 0.011</u>	99.95 ± 0.010	<u>99.96 ± 0.011</u>	<u>99.96 ± 0.011</u>	99.99 ± 0.004	99.95 ± 0.013
	MNIST-c	<u>89.53 ± 0.560</u>	89.26 ± 0.538	89.38 ± 0.569	89.25 ± 0.606	90.22 ± 0.577	89.51 ± 0.469
FMNIST	ACC	92.38 ± 0.194	92.45 ± 0.211	<u>92.40 ± 0.197</u>	92.36 ± 0.198	92.35 ± 0.117	92.25 ± 0.238
	NLL	0.226 ± 0.005	0.225 ± 0.006	0.223 ± 0.005	<u>0.224 ± 0.006</u>	0.223 ± 0.005	0.230 ± 0.006
	MNIST	<u>99.70 ± 0.170</u>	99.83 ± 0.085	91.31 ± 1.356	90.47 ± 1.766	99.05 ± 0.271	97.11 ± 1.063
	NotMNIST	<u>96.23 ± 0.665</u>	96.96 ± 0.724	89.32 ± 1.844	89.07 ± 1.697	95.31 ± 0.679	93.36 ± 0.630
CIFAR-10	ACC	87.17 ± 0.382	86.88 ± 0.612	86.81 ± 0.680	<u>86.95 ± 0.412</u>	86.52 ± 0.395	86.73 ± 0.349
	NLL	0.380 ± 0.010	0.393 ± 0.015	0.393 ± 0.019	<u>0.391 ± 0.009</u>	0.398 ± 0.013	0.402 ± 0.010
	SVHN	84.22 ± 2.104	84.40 ± 2.170	83.22 ± 3.230	<u>84.18 ± 0.913</u>	<u>84.87 ± 2.269</u>	86.51 ± 2.022
	CIFAR-10C0	55.59 ± 0.539	55.30 ± 0.447	55.50 ± 0.676	55.38 ± 0.603	<u>55.34 ± 0.429</u>	55.58 ± 0.466
	CIFAR-10C2	<u>64.82 ± 1.007</u>	64.34 ± 0.803	64.64 ± 1.293	64.33 ± 1.175	64.19 ± 0.784	65.02 ± 0.895
	CIFAR-10C4	<u>72.15 ± 1.471</u>	71.87 ± 1.268	71.72 ± 1.906	71.46 ± 1.454	71.35 ± 1.225	72.55 ± 1.507
PathMNIST	ACC	87.57 ± 1.326	87.78 ± 1.154	88.08 ± 1.237	<u>88.02 ± 1.012</u>	87.83 ± 1.143	88.01 ± 1.093
	NLL	0.470 ± 0.110	0.423 ± 0.044	<u>0.424 ± 0.050</u>	0.458 ± 0.050	0.454 ± 0.069	0.441 ± 0.046
	BloodMNIST	97.35 ± 1.720	96.97 ± 1.317	97.69 ± 0.973	<u>97.43 ± 1.179</u>	97.29 ± 0.957	97.14 ± 2.531
OrganAMNIST	ACC	<u>90.50 ± 0.531</u>	90.16 ± 0.635	90.35 ± 0.273	89.65 ± 0.877	90.37 ± 0.937	90.55 ± 0.496
	NLL	<u>0.305 ± 0.016</u>	0.317 ± 0.012	0.314 ± 0.008	0.354 ± 0.022	0.316 ± 0.028	0.297 ± 0.011
	OrganSMNIST	81.90 ± 0.800	87.85 ± 2.960	89.86 ± 2.058	80.20 ± 0.948	83.16 ± 2.210	<u>87.93 ± 1.208</u>

rotational transformations to the test data without applying such transformations during training, thereby evaluating the generalisation ability of our proposed method to unseen rotations. Figure 1 shows the ACC and NLL performance of ST-FS-EB and baseline methods under distribution shift on MNIST, FMNIST, and CIFAR-10, while the results for PathMNIST and OrganAMNIST are reported in Figure 2 (Section C.1)). The results demonstrate that the proposed method consistently achieves higher ACC and lower NLL than competing approaches, with only marginal differences compared to MC Dropout in a few scenarios. This highlights the strong robustness of ST-FS-EB under distribution shifts compared with existing baselines, which is critical for safety-sensitive and real-world deployment scenarios.

5.3 INFLUENCE OF DEGREES OF FREEDOM IN THE STUDENT-T PRIOR

This experiment studies the influence of the dof parameter of Student’s t priors on the performance of ST-FS-EB. We evaluate a range of dof values [2.1, 3.0, 5.0, 10.0, 20.0] and additionally include a Gaussian prior. The experimental results are summarised in Table 3. The optimal dof value exhibits clear dataset dependence for both in-distribution prediction (ACC and NLL) and OOD detection performance. For in-distribution prediction evaluation, no single dof value consistently dominates across datasets. On MNIST and FMNIST, higher dof (dof = 5.0–20.0) generally yield slightly better ACC and NLL performance. On CIFAR-10, dof = 2.1 achieves the optimal results, indicating a preference for

heavier-tailed priors. For PathMNIST, dof = 5.0 provides the best performance. In contrast, on OrganAMNIST, the Gaussian prior attains optimal predictive performance. A similar pattern is observed for OOD detection. The best-performing dof configurations vary across benchmarks. For instance, dof = 20.0 performs the best on MNIST-based OOD tasks, while dof = 3.0 is optimal for FMNIST-based OOD detection. The Gaussian prior remains competitive in CIFAR-10, while dof = 5.0 is generally favourable for PathMNIST and OrganAMNIST. These observations demonstrate that the proposed heavy-tailed Student’s t prior assumption provides meaningful modelling flexibility for real-world data, yielding gains in both predictive accuracy and OOD detection.

6 CONCLUSION

This paper proposes ST-FS-EB, a Student’s t -based function-space empirical Bayes regularisation framework, which introduces heavy-tailed priors over both parameter and functional distributions. We further derive an MC dropout-based ELBO objective to enable scalable posterior inference. The proposed method is compared with several baseline methods, and experiment results show that ST-FS-EB achieves a superior balance between predictive accuracy and OOD detection performance. Also, the ST-FS-EB exhibits the most robust performance under distribution shifts. Moreover, the optimal dof values of the Student’s t priors are dataset-dependent, and Student’s t priors present better prediction and OOD detection performance than Gaussian priors in most cases.

References

- Mohammad Ahsanullah, BM Golam Kibria, and Mohammad Shakil. *Normal and student's t distributions and their applications*, volume 4. Springer, 2014.
- Christopher M Bishop and Nasser M Nasrabadi. *Pattern recognition and machine learning*, volume 4. Springer, 2006.
- Charles Blundell, Julien Cornebise, Koray Kavukcuoglu, and Daan Wierstra. Weight uncertainty in neural network. In *International conference on machine learning*, pages 1613–1622. PMLR, 2015.
- David R. Burt, Sebastian W. Ober, Adrià Garriga-Alonso, and Mark van der Wilk. Understanding variational inference in function-space. In *Third Symposium on Advances in Approximate Bayesian Inference*, 2021. URL <https://openreview.net/forum?id=7P9y3sRa5Mk>.
- Tristan Cinqun and Robert Bamler. Regularized KL-divergence for well-defined function-space variational inference in bayesian neural networks. In *ICML 2024 Workshop on Structured Probabilistic Inference & Generative Modeling*, 2024. URL <https://openreview.net/forum?id=vwfWsUKW7E>.
- Daniel Flam-Shepherd, James Requeima, and David Duvenaud. Mapping gaussian process priors to bayesian neural networks. In *NIPS Bayesian deep learning workshop*, volume 3, 2017.
- Vincent Fortuin, Adrià Garriga-Alonso, Mark van der Wilk, and Laurence Aitchison. Bnnpriors: A library for bayesian neural network inference with different prior distributions. *Software Impacts*, 9:100079, 2021.
- Vincent Fortuin, Adrià Garriga-Alonso, Sebastian W. Ober, Florian Wenzel, Gunnar Ratsch, Richard E Turner, Mark van der Wilk, and Laurence Aitchison. Bayesian neural network priors revisited. In *International Conference on Learning Representations*, 2022. URL <https://openreview.net/forum?id=xkjQJYqRJy>.
- Yarin Gal and Zoubin Ghahramani. Dropout as a bayesian approximation: Representing model uncertainty in deep learning. In *international conference on machine learning*, pages 1050–1059. PMLR, 2016.
- Jakob Gawlikowski, Cedrique Rovile Njiteucheu Tassi, Mohsin Ali, Jongseok Lee, Matthias Humt, Jianxiang Feng, Anna Kruspe, Rudolph Triebel, Peter Jung, Ribana Roscher, et al. A survey of uncertainty in deep neural networks. *Artificial intelligence review*, 56(Suppl 1): 1513–1589, 2023.
- Alex Graves. Practical variational inference for neural networks. *Advances in neural information processing systems*, 24, 2011.
- James Harrison, John Willes, Paul Brunzema, and Jasper Snoek. Heteroscedastic variational last layers. In *7th Symposium on Advances in Approximate Bayesian Inference* {\textdash} Workshop Track, 2025.
- Geoffrey E Hinton and Drew Van Camp. Keeping the neural networks simple by minimizing the description length of the weights. In *Proceedings of the sixth annual conference on Computational learning theory*, pages 5–13, 1993.
- Alexander Immer, Maciej Korzepa, and Matthias Bauer. Improving predictions of bayesian neural nets via local linearization. In *International conference on artificial intelligence and statistics*, pages 703–711. PMLR, 2021.
- Laurent Valentin Jospin, Hamid Laga, Farid Boussaid, Wray Buntine, and Mohammed Bennamoun. Hands-on bayesian neural networks—a tutorial for deep learning users. *IEEE Computational Intelligence Magazine*, 17(2): 29–48, 2022.
- Mohammad Emtiyaz Khan, Alexander Immer, Ehsan Abedi, and Maciej Korzepa. Approximate inference turns deep networks into gaussian processes. *Advances in neural information processing systems*, 32, 2019.
- Diederik P Kingma and Max Welling. Auto-encoding variational bayes. In *International Conference on Learning Representations (ICLR)*, 2014. URL <https://openreview.net/forum?id=33X9fd2-9FyZd>.
- Benjamin Lambert, Florence Forbes, Senan Doyle, Harmonie Dehaene, and Michel Dojat. Trustworthy clinical ai solutions: a unified review of uncertainty quantification in deep learning models for medical image analysis. *Artificial Intelligence in Medicine*, 150:102830, 2024.
- Chao Ma and José Miguel Hernández-Lobato. Functional variational inference based on stochastic process generators. *Advances in Neural Information Processing Systems*, 34:21795–21807, 2021.
- Chao Ma, Yingzhen Li, and José Miguel Hernández-Lobato. Variational implicit processes. In *International Conference on Machine Learning*, pages 4222–4233. PMLR, 2019.
- Dimitrios Milios, Raffaello Camoriano, Pietro Michiardi, Lorenzo Rosasco, and Maurizio Filippone. Dirichlet-based gaussian processes for large-scale calibrated classification. *Advances in Neural Information Processing Systems*, 31, 2018.
- Tim G. J. Rudner, Sanyam Kapoor, Shikai Qiu, and Andrew Gordon Wilson. Function-space regularization in neural networks: A probabilistic perspective. In *Fifth Symposium on Advances in Approximate Bayesian Inference*

- *Fast Track*, 2023. URL <https://openreview.net/forum?id=T9X1kS5FIk>.
- Tim G. J. Rudner, Xiang Pan, Yucen Lily Li, Ravid Shwartz-Ziv, and Andrew Gordon Wilson. Fine-tuning with uncertainty-aware priors makes vision and language foundation models more reliable. In *ICML 2024 Workshop on Structured Probabilistic Inference & Generative Modeling*, 2024a. URL <https://openreview.net/forum?id=37fM2QEBSSE>.
- Tim GJ Rudner, Zonghao Chen, Yee Whye Teh, and Yarin Gal. Tractable function-space variational inference in bayesian neural networks. *Advances in Neural Information Processing Systems*, 35:22686–22698, 2022.
- Tim GJ Rudner, Xiang Pan, Yucen Lily Li, Ravid Shwartz-Ziv, and Andrew Gordon Wilson. Fine-tuning with uncertainty-aware priors makes vision and language foundation models more reliable. In *ICML 2024 Workshop on Structured Probabilistic Inference & Generative Modeling*, 2024b.
- Tim GJ Rudner, Ya Shi Zhang, Andrew Gordon Wilson, and Julia Kempe. Mind the gap: Improving robustness to subpopulation shifts with group-aware priors. In *International Conference on Artificial Intelligence and Statistics*, pages 127–135. PMLR, 2024c.
- Matthias Seeger. Gaussian processes for machine learning. *International journal of neural systems*, 14(02):69–106, 2004.
- Amar Shah, Andrew Wilson, and Zoubin Ghahramani. Student-t processes as alternatives to gaussian processes. In *Artificial intelligence and statistics*, pages 877–885. PMLR, 2014.
- Jiaxin Shi, Shengyang Sun, and Jun Zhu. A spectral approach to gradient estimation for implicit distributions. In *International Conference on Machine Learning*, pages 4644–4653. PMLR, 2018.
- Arno Solin and Simo Särkkä. State space methods for efficient inference in student-t process regression. In *Artificial Intelligence and Statistics*, pages 885–893. PMLR, 2015.
- Shengyang Sun, Guodong Zhang, Jiaxin Shi, and Roger Grosse. FUNCTIONAL VARIATIONAL BAYESIAN NEURAL NETWORKS. In *International Conference on Learning Representations*, 2019. URL <https://openreview.net/forum?id=rkxacs0qY7>.
- Ke Wang, Chongqiang Shen, Xingcan Li, and Jianbo Lu. Uncertainty quantification for safe and reliable autonomous vehicles: A review of methods and applications. *IEEE Transactions on Intelligent Transportation Systems*, 2025.
- Ziyu Wang, Tongzheng Ren, Jun Zhu, and Bo Zhang. Function space particle optimization for bayesian neural networks. In *International Conference on Learning Representations*, 2019. URL <https://openreview.net/forum?id=BkgtDsCcKQ>.
- Andrew G Wilson and Pavel Izmailov. Bayesian deep learning and a probabilistic perspective of generalization. *Advances in neural information processing systems*, 33:4697–4708, 2020.
- Xuanzhe Xiao, Zeng Li, Chuanlong Xie, and Fengwei Zhou. Heavy-tailed regularization of weight matrices in deep neural networks. In *International Conference on Artificial Neural Networks*, pages 236–247. Springer, 2023.

Function-Space Empirical Bayes Regularisation with Student's t Priors (Supplementary Material)

Pengcheng Hao¹

Ercan Engin Kuruoglu¹

¹Institute of Data and Information, Tsinghua Shenzhen International Graduate School, Shenzhen, China

A THE EMPIRICAL BAYES VARIATIONAL OBJECTIVE VIA MC DROPOUT

In this section, we derive the proposed ST-FS-EB variational objective. Starting from Eq. (13), we obtain:

$$\begin{aligned}\mathcal{L}(\boldsymbol{\theta}) &= \mathbb{E}_{q(\boldsymbol{\theta})} [\log p(\mathbf{y}_{\mathcal{D}} | \mathbf{x}_{\mathcal{D}}, \boldsymbol{\theta})] - D_{\text{KL}}(q(\boldsymbol{\theta}) \| p_{st}(\boldsymbol{\theta} | \mathbf{y}_c, \mathbf{x}_c)) \\ &= \mathbb{E}_{q(\boldsymbol{\theta})} [\log p(\mathbf{y}_{\mathcal{D}} | \mathbf{x}_{\mathcal{D}}, \boldsymbol{\theta})] + \int q(\boldsymbol{\theta}) \log \frac{p_{st}(\boldsymbol{\theta} | \mathbf{y}_c, \mathbf{x}_c)}{q(\boldsymbol{\theta})} d\boldsymbol{\theta}\end{aligned}$$

Substituting the ST-FS-EB prior in Eq. (12) into the objective, we obtain

$$\begin{aligned}\mathcal{L}(\boldsymbol{\theta}) &\propto \mathbb{E}_{q(\boldsymbol{\theta})} [\log p(\mathbf{y}_{\mathcal{D}} | \mathbf{x}_{\mathcal{D}}, \boldsymbol{\theta})] + \int q(\boldsymbol{\theta}) \log \frac{\prod_{i=1}^{\mathcal{I}} p_{st}(\theta_i) \prod_{l=1}^L p_{st}(\mathbf{y}_c^l | \mathbf{x}_c, \boldsymbol{\theta})}{q(\boldsymbol{\theta})} d\boldsymbol{\theta} \\ &= \mathbb{E}_{q(\boldsymbol{\theta})} [\log p(\mathbf{y}_{\mathcal{D}} | \mathbf{x}_{\mathcal{D}}, \boldsymbol{\theta})] + \sum_{l=1}^L \mathbb{E}_{q(\boldsymbol{\theta})} [\log p_{st}(\mathbf{y}_c^l | \mathbf{x}_c, \boldsymbol{\theta})] + \sum_{i=1}^{\mathcal{I}} \mathbb{E}_{q(\boldsymbol{\theta})} (\log p_{st}(\theta_i)) - \mathbb{E}_{q(\boldsymbol{\theta})} (q(\boldsymbol{\theta}))\end{aligned}$$

To enable a tractable VI formulation, we parameterise the variational distribution $q(\boldsymbol{\theta})$ using MC dropout. Under this approximation, the entropy term $\mathbb{E}_{q(\boldsymbol{\theta})} (q(\boldsymbol{\theta}))$ becomes a constant Gal and Ghahramani [2016]. Let ρ denotes the dropout rate, we have

$$\mathcal{L}(\boldsymbol{\theta}) \propto \frac{1}{S} \sum_{s=1}^S \left[\log p(\mathbf{y}_{\mathcal{D}} | \mathbf{x}_{\mathcal{D}}, \boldsymbol{\theta}^{(s)}) + \sum_{l=1}^L \log p_{st}(\mathbf{y}_c^l | \mathbf{x}_c, \boldsymbol{\theta}^{(s)}) \right] + \rho \sum_{i=1}^{\mathcal{I}} \log p_{st}(\theta_i)$$

where $\boldsymbol{\theta}^{(s)} \sim q(\boldsymbol{\theta})$ denotes the effective parameters associated with the s -th dropout mask. By Eq. (11), we have

$$\log p_{st}(\mathbf{y}_c^l | \mathbf{x}_c, \boldsymbol{\theta}^{(s)}) = \log \mathcal{MVT}(\mathbf{y}_c^l; \nu_{\theta}, [f(\mathbf{x}_c; \boldsymbol{\theta})]_l, \mathbf{K}(\mathbf{x}_c, \mathbf{x}_c))$$

Let $\mathbf{y}_c^l = \mathbf{0}$, then

$$\begin{aligned}& \log p_{st}(\mathbf{y}_c^l | \mathbf{x}_c, \boldsymbol{\theta}^{(s)}) \\ &= \log \mathcal{MVT}(\mathbf{y}_c^l; \nu_{\theta}, [f(\mathbf{x}_c; \boldsymbol{\theta}^{(s)})]_l, \mathbf{K}(\mathbf{x}_c, \mathbf{x}_c)) \\ &= \log \left[\frac{\Gamma(\frac{\nu_{\theta} + N_c}{2})}{\Gamma(\frac{\nu_{\theta}}{2}) ((\nu_{\theta} - 2)\pi)^{N_c/2}} |\mathbf{K}(\mathbf{x}_c, \mathbf{x}_c)|^{-1/2} \left(1 + \frac{[f(\mathbf{x}_c; \boldsymbol{\theta}^{(s)})]_l^{\top} \mathbf{K}^{-1}(\mathbf{x}_c, \mathbf{x}_c) [f(\mathbf{x}_c; \boldsymbol{\theta}^{(s)})]_l}{\nu_{\theta} - 2} \right)^{-\frac{\nu_{\theta} + N_c}{2}} \right] \\ &= \log \left[\frac{\Gamma(\frac{\nu_{\theta} + N_c}{2})}{\Gamma(\frac{\nu_{\theta}}{2}) ((\nu_{\theta} - 2)\pi)^{N_c/2}} \right] - \frac{1}{2} \log |\mathbf{K}(\mathbf{x}_c, \mathbf{x}_c)| - \frac{\nu_{\theta} + N_c}{2} \log \left(1 + \frac{[f(\mathbf{x}_c; \boldsymbol{\theta}^{(s)})]_l^{\top} \mathbf{K}^{-1}(\mathbf{x}_c, \mathbf{x}_c) [f(\mathbf{x}_c; \boldsymbol{\theta}^{(s)})]_l}{\nu_{\theta} - 2} \right) \\ &\propto -\frac{\nu_{\theta} + N_c}{2} \log \left(1 + \frac{[f(\mathbf{x}_c; \boldsymbol{\theta}^{(s)})]_l^{\top} \mathbf{K}^{-1}(\mathbf{x}_c, \mathbf{x}_c) [f(\mathbf{x}_c; \boldsymbol{\theta}^{(s)})]_l}{\nu_{\theta} - 2} \right)\end{aligned}$$

Also, according to (1) and (10), $\log p_{st}(\theta_i)$ can be calculated by

$$\begin{aligned} \log p_{st}(\theta_i) &= \log \mathcal{ST}(\theta_i; \nu_\theta, 0, \sigma_\theta^2) \\ &= \log \left[\frac{\Gamma(\frac{\nu_\theta+1}{2})}{\Gamma(\frac{\nu_\theta}{2}) \sqrt{\pi \nu_\theta \sigma_\theta^2}} \left(1 + \frac{\theta_i^2}{\nu_\theta \sigma_\theta^2}\right)^{-\frac{\nu_\theta+1}{2}} \right] \\ &= \log \left[\frac{\Gamma(\frac{\nu_\theta+1}{2})}{\Gamma(\frac{\nu_\theta}{2}) \sqrt{\pi \nu_\theta \sigma_\theta^2}} \right] - \frac{\nu_\theta+1}{2} \log \left(1 + \frac{\theta_i^2}{\nu_\theta \sigma_\theta^2}\right) \\ &\propto -\frac{\nu_\theta+1}{2} \log \left(1 + \frac{\theta_i^2}{\nu_\theta \sigma_\theta^2}\right) \end{aligned}$$

Following this, we have our ST-FS-BE VI objective:

$$\begin{aligned} \mathcal{L}(\boldsymbol{\theta}) &\propto \frac{1}{S} \sum_{s=1}^S \left[\log p(\mathbf{y}_D | \mathbf{x}_D, \boldsymbol{\theta}^{(s)}) + \sum_{l=1}^L \log p_{st}(\mathbf{y}_c^l | \mathbf{x}_c, \boldsymbol{\theta}^{(s)}) \right] + \rho \sum_{i=1}^{\mathcal{I}} \log p_{st}(\theta_i) \\ &\propto \frac{1}{S} \sum_{s=1}^S \left[\log p(\mathbf{y}_D | \mathbf{x}_D, \boldsymbol{\theta}^{(s)}) - \frac{\nu_\theta + N_c}{2} \sum_{l=1}^L \log \left(1 + \frac{[f(\mathbf{x}_c; \boldsymbol{\theta}^{(s)})]_l^\top \mathbf{K}^{-1}(\mathbf{x}_c, \mathbf{x}_c) [f(\mathbf{x}_c; \boldsymbol{\theta}^{(s)})]_l}{\nu_\theta - 2} \right) \right] \\ &\quad - \frac{\rho(\nu_\theta + 1)}{2} \sum_{i=1}^{\mathcal{I}} \log \left(1 + \frac{\theta_i^2}{\nu_\theta \sigma_\theta^2} \right) \end{aligned}$$

B ADDITIONAL EXPERIMENTAL DETAILS

B.1 HYPERPARAMETERS

Table 4 outlines the search space for the key hyperparameters of our proposed ST-FS-EB method. We perform hyperparameter optimisation using randomised search over this space, running a total of 300 trials for each experiment. The best configuration is chosen based on the lowest NLL achieved on the validation set. All experiments employ early stopping with a maximum of 100 training epochs and a patience of 10 epochs. Additionally, the models are trained across all tasks using the Adam optimiser with a learning rate of 5×10^{-4} , a numerical stability parameter $\epsilon_1 = 10^{-8}$, momentum parameters $(\beta_1, \beta_2) = (0.9, 0.999)$, and a batch size of 128. Context points are sampled from the context datasets, and unless otherwise specified, their number N_c^m is fixed at 32. During training, we use $S = 10$ MC samples from $q(\boldsymbol{\theta})$ to approximate the objective; at inference, predictions are averaged over $\Xi = 10$ stochastic forward passes to estimate the predictive distribution.

Table 4: Hyperparameter Ranges

Hyperparameters	Range
ν_θ	{2.1, 3.0, 5.0, 10.0, 20.0}
σ_θ	{ 10^ℓ $\ell = -6, -5, \dots, 1$ }
τ_1	{ 10^ℓ $\ell = -6, -5, \dots, 2$ }
τ_2	{ 10^ℓ $\ell = -6, -5, \dots, 2$ }

To ensure a fair and consistent comparison, all baseline methods employ the same optimiser and training protocol—including batch size, learning rate, early stopping criterion and so on. The FS-EB derives the empirical prior from a randomly initialised neural network, consistent with the findings of Wilson et al. Wilson and Izmailov [2020]. In GFSVI, we use a GP prior with a constant zero-mean function, where the covariance kernel hyperparameters are optimised via mini-batch log marginal likelihood maximisation, as in Miliotis et al. Miliotis et al. [2018]. Both FS-EB and GFSVI draw their context points from the same context datasets used by ST-FS-EB. Finally, for MC Dropout, MFVI, and MAP methods, the isotropic Gaussian weight prior parameters are chosen using a random search procedure.

B.2 MNIST, FMNIST AND ORGANAMNIST

For MNIST, FMNIST and OrganAMNIST datasets, we adopt a convolutional neural network architecture consisting of two convolutional layers with 32 and 64 filters of size 3×3 , respectively. Each convolutional layer is followed by a ReLU

activation and a max-pooling operation. The feature representations are flattened and fed into a fully connected layer with 128 hidden units, before a final linear layer produces the classification outputs. For MC Dropout-based methods, dropout layers are placed after each convolutional block and the fully connected layer, and remain active at inference time to facilitate MC sampling. The dropout rate is set to 0.5 for MNIST and FashionMNIST, and to 0.3 for OrganAMNIST. For MNIST and FashionMNIST, Kuzushiji-MNIST (KMNIST) is used as the context dataset, whereas OrganCMNIST is used as the context dataset for OrganAMNIST. For MNIST and FMNIST, 10% of the training set is held out as a validation set, while for OrganAMNIST, its own validation set is used.

B.3 CIFAR-10 AND PATHMNIST

For both CIFAR-10 and PathMNIST datasets, we employ a convolutional neural network comprising six convolutional layers with 32, 32, 64, 64, 128, and 128 filters, each of size 3×3 . ReLU activation functions follow each convolutional layer, while max-pooling layers are applied after the second, fourth, and sixth convolutional layers to progressively reduce the spatial dimensions. The extracted feature maps are flattened and processed by a fully connected layer with 128 hidden units, after which a linear layer produces the final classification outputs. In MC Dropout-based methods, dropout is applied after each convolutional block and the fully connected layer, remaining active at inference to enable MC sampling. The dropout rate is set to 0.1 for both CIFAR-10 and PathMNIST. CIFAR-100 is used as the context dataset for CIFAR-10, while DermaMNIST serves as the context dataset for PathMNIST. For CIFAR-10, 10% of the training set is held out as a validation set, whereas PathMNIST uses its provided validation split. For both datasets, data augmentation is performed by applying random horizontal flips with a 50% probability, followed by random cropping with a padding of 4 pixels on all sides.

C ADDITIONAL SIMULATION RESULTS

C.1 ADDITIONAL RESULTS UNDER DISTRIBUTION SHIFTS

Following the experimental results presented in Section 5.2, this section reports additional evaluations under distribution shift. Figure 2 presents the ACC and NLL performance of ST-FS-EB and the baseline methods on PathMNIST and OrganMNIST under the controlled rotational transformations. The results demonstrate that ST-FS-EB consistently achieves superior classification accuracy and lower NLL compared to most competing methods. Although its NLL is higher than that of MFVI and MAP on PathMNIST, ST-FS-EB outperforms the other functional regularisation-based approaches.

C.2 INFLUENCE OF THE NUMBER OF CONTEXT POINTS

This experiment investigates the impact of the number of context points on model performance. We adopt the same experimental setup as in Section 5.1, and Table 5 reports the results across multiple datasets and evaluation metrics. The results indicate that the model is insensitive to the choice of context numbers $\{32, 64, 128\}$, with only marginal variations observed in ACC, NLL and OOD detection performance. This indicates that the proposed method does not depend critically on a specific number of context points and remains robust across different context sizes.

C.3 INFLUENCE OF TRAINING CONTEXT DISTRIBUTIONS

This experiment investigates the impact of the context distributions on model performance. We adopt the same experimental setup as in Section 5.1 and consider two types of context points: (i) samples drawn from the training batches (TRAIN), and (ii) samples drawn from auxiliary context datasets x_c , as defined in Section 5 and Section B. Table 6 reports the results across multiple datasets and evaluation metrics. When context points are sampled from the training dataset (TRAIN), the model consistently achieves higher ACC scores. In contrast, using auxiliary datasets leads to a slight degradation in ACC. However, this reduction is accompanied by improved uncertainty qualification, reflected by lower ECE and NLL, as well as substantially better OOD detection performance. These results indicate that auxiliary context datasets enable a more favourable trade-off between predictive accuracy and uncertainty quantification.

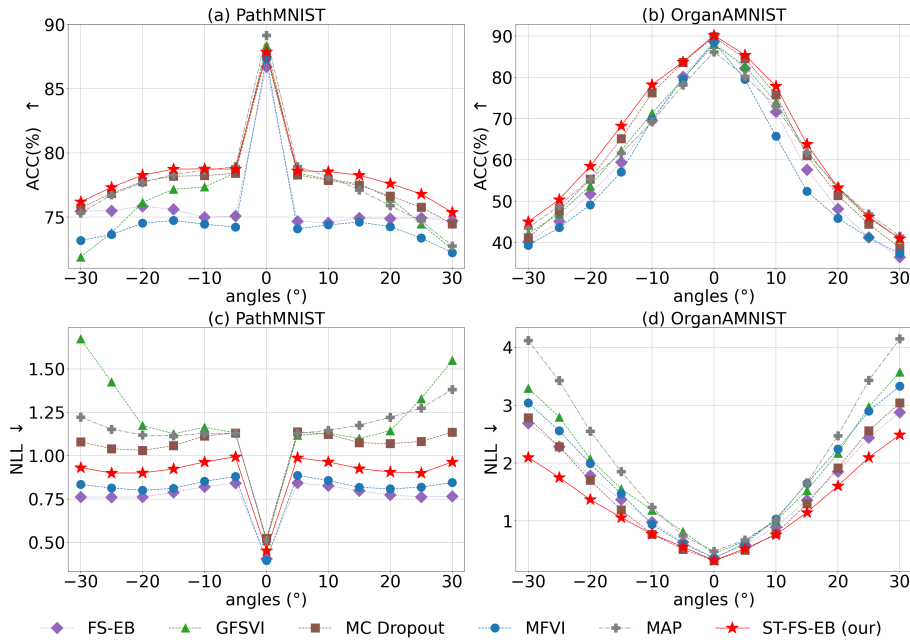


Figure 2: Performance under distribution shift induced by image rotations. The top row ((a) (b)) reports ACC scores, while the bottom row ((c) (d)) shows NLL. The horizontal axes denote the rotation angle, ranging from -30° to 30° , and the vertical axis shows the corresponding performance scores.

C.4 TRAINING EFFICIENCY

This experiment investigates the training efficiency of the proposed method. We adopt the same experimental setup as in Section 5.1. Table 7 shows the average per-epoch training time and memory consumption of ST-FS-EB in comparison with various baselines across multiple datasets. ST-FS-EB incurs a higher computational cost than traditional weight-space regularisation methods, such as MFVI and MAP, reflecting the additional overhead introduced by functional regularisation. However, compared to other function-space approaches (FS-EB and GFSVI), ST-FS-EB is substantially more efficient, requiring less training time and lower memory usage across all benchmarks. This efficiency advantage arises from two factors: 1) ST-FS-EB avoids linearisation-based approximations, thereby eliminating the computational burden of Jacobian evaluations; 2) the use of MC dropout induces sparsity in the network structure, which reduces both computational and memory costs during training.

Table 5: Influence of the number of context points. **Best** results are in bold. OOD detection evaluation: for MNIST, OOD1 = FashionMNIST and OOD2 = NotMNIST; for FashionMNIST, OOD1 = MNIST and OOD2 = NotMNIST; for CIFAR-10, OOD1 = SVHN and OOD2 = CIFAR-10C0; for PathMNIST, OOD1=BloodMNIST; for OrganAMNIST, OOD1=OrganSMNIST.

Metric	Context number	MNIST	FMNIST	CIFAR-10	PathMNIST	OrganAMNIST
ACC	32	99.33 ± 0.052	92.38 ± 0.194	86.52 ± 0.395	87.83 ± 1.143	90.16 ± 0.635
	64	99.31 ± 0.035	92.42 ± 0.268	86.57 ± 0.429	87.02 ± 1.346	90.60 ± 0.457
	128	99.33 ± 0.047	92.35 ± 0.218	86.66 ± 0.245	87.78 ± 1.353	90.65 ± 0.386
NLL	32	0.028 ± 0.001	0.226 ± 0.005	0.398 ± 0.013	0.454 ± 0.069	0.317 ± 0.012
	64	0.029 ± 0.002	0.229 ± 0.007	0.398 ± 0.012	0.448 ± 0.066	0.297 ± 0.017
	128	0.030 ± 0.002	0.230 ± 0.006	0.399 ± 0.007	0.437 ± 0.052	0.291 ± 0.013
OOD1	32	99.86 ± 0.057	99.86 ± 0.057	84.87 ± 2.269	97.29 ± 0.957	87.85 ± 2.960
	64	99.92 ± 0.022	99.85 ± 0.066	86.41 ± 2.526	96.79 ± 1.176	83.15 ± 1.200
	128	99.98 ± 0.005	99.69 ± 0.141	86.60 ± 1.963	97.25 ± 1.896	84.50 ± 1.004
OOD2	32	99.96 ± 0.011	96.23 ± 0.665	71.35 ± 1.225	–	–
	64	99.97 ± 0.013	97.17 ± 0.616	72.01 ± 1.533	–	–
	128	99.99 ± 0.003	96.45 ± 0.676	72.64 ± 1.271	–	–

Table 6: Influence of the context distributions. **Best** results are in bold. OOD detection evaluation: for MNIST, OOD1 = FashionMNIST and OOD2 = NotMNIST; for FashionMNIST, OOD1 = MNIST and OOD2 = NotMNIST; for CIFAR-10, OOD1 = SVHN and OOD2 = CIFAR-10C0; for PathMNIST, OOD1=BloodMNIST; for OrganAMNIST, OOD1=OrganSMNIST.

Dataset	Setting	ACC	ECE	NLL	OOD1	OOD2
MNIST	TRAIN	99.37 ± 0.048	0.015 ± 0.001	0.032 ± 0.001	99.22 ± 0.156	97.99 ± 0.460
	x_c	99.33 ± 0.052	0.012 ± 0.001	0.028 ± 0.001	99.86 ± 0.057	99.96 ± 0.011
FMNIST	TRAIN	92.43 ± 0.237	0.039 ± 0.004	0.226 ± 0.005	85.56 ± 2.097	81.62 ± 2.170
	x_c	92.38 ± 0.194	0.038 ± 0.003	0.226 ± 0.005	99.70 ± 0.170	96.23 ± 0.665
CIFAR-10	TRAIN	86.53 ± 0.445	0.027 ± 0.006	0.400 ± 0.013	84.97 ± 2.594	71.95 ± 1.478
	x_c	86.52 ± 0.395	0.021 ± 0.007	0.398 ± 0.013	84.87 ± 2.269	71.35 ± 1.225
PathMNIST	TRAIN	88.18 ± 1.160	0.053 ± 0.009	0.492 ± 0.156	76.23 ± 22.597	–
	x_c	87.83 ± 1.143	0.049 ± 0.009	0.454 ± 0.069	97.29 ± 0.957	–
OrganAMNIST	TRAIN	91.21 ± 0.382	0.016 ± 0.002	0.276 ± 0.008	82.13 ± 0.469	–
	x_c	90.16 ± 0.635	0.026 ± 0.007	0.317 ± 0.012	87.85 ± 2.960	–

Table 7: Training time and memory.

Metric	Dataset	ST-FS-EB(our)	FS-EB	GFSVI	MC Dropout	MFVI	MAP
Time (s/epoch) ↓	MNIST	18.52	26.96	40.44	11.24	18.13	17.86
	FMNIST	18.10	26.63	40.76	11.17	17.87	17.62
	CIFAR-10	43.89	58.69	93.01	32.09	44.39	18.45
	PathMNIST	74.34	97.36	136.86	52.39	71.82	45.63
	OrganAMNIST	20.42	25.33	35.62	16.04	22.02	15.24
Memory (MB) ↓	MNIST	536.14	808.39	1055.66	437.84	633.32	67.09
	FMNIST	536.14	808.39	1055.66	437.84	633.32	67.09
	CIFAR-10	1590.82	2060.54	2605.42	1275.60	1714.07	112.83
	PathMNIST	1225.31	1745.45	2098.75	983.55	1479.45	93.06
	OrganAMNIST	535.58	807.85	1096.22	437.28	632.76	67.09